Journal of Applied Physics

Illusion thermotics with topology optimization

Cite as: J. Appl. Phys. **128**, 045106 (2020); https://doi.org/10.1063/5.0007354
Submitted: 13 March 2020 . Accepted: 03 July 2020 . Published Online: 23 July 2020

Wei Sha, Yiting Zhao, Liang Gao, Mi Xiao, and Run Hu

Journal of Applied Physics ARTICLE scitation.org/journal/jap

Illusion thermotics with topology optimization

Cite as: J. Appl. Phys. **128**, 045106 (2020); doi: 10.1063/5.0007354
Submitted: 13 March 2020 · Accepted: 3 July 2020 ·
Published Online: 23 July 2020

Wei Sha,[1] Yiting Zhao,[2] Liang Gao,[1] Mi Xiao,[1,a)] and Run Hu[2,3,a)]

AFFILIATIONS

[1]State Key Laboratory of Digital Manufacturing Equipment and Technology, Huazhong University of Science and Technology, Wuhan 430074, China
[2]China-EU Institute for Clean and Renewable Energy, Huazhong University of Science and Technology, Wuhan 430074, China
[3]School of Energy and Power Engineering, Huazhong University of Science and Technology, Wuhan 430074, China

[a)]**Authors to whom correspondence should be addressed:** xiaomi@hust.edu.cn and hurun@hust.edu.cn

ABSTRACT

Illusion thermotics, which aims at creating temperature fields to mislead a thermal detector, encompasses many thermal functionalities. It has attracted significant attention due to the increasing number of promising applications. Transformation thermotics and scattering cancellation methods are frequently adopted for illusion devices, though they have inherent defects such as anisotropic thermal properties and complicated fabrication methods. Here, we present a general framework for topology optimization, which can be used to design the structure of an illusion device automatically. The optimized configuration can camouflage the thermal exterior of an illusion device so that it is identical to a reference. The original heat source can drive the virtual heat source despite the structure being simply composed of natural materials. To establish an effective topology optimization model, a volume constraint was imposed on the total volume of iron and a prescribed objective function was used to evaluate the difference between the reference temperature and the temperature field during the topology optimization. The flexibility of the method presented was successfully validated by changing the total volume of iron, the number and locations of the thermal illusions, the types of composite materials, and the original heat sources. Topology optimization is a new and flexible approach for designing thermal metamaterials and metadevices for diverse thermal functionalities and beyond.

I. INTRODUCTION

With the advent of thermal metamaterials in recent decades, many novel thermal functionalities have been proposed and there is an increasing number of promising applications, including thermal cloaking,[1–9] thermal concentrating,[1,10,11] thermal camouflage,[12] thermal illusion,[13,14] etc. Illusion thermotics, which uses thermal metamaterials and metadevices to create thermal illusions, encompasses all these thermal functionalities. Generally, if there is no thermal reference, then the illusion thermotics could include thermal cloaking, whereas if the reference is part of the background, then the illusion thermotics could include thermal camouflage. Transformation thermotics (TT) and scattering cancellation (SC) methods are frequently adopted to design thermal metadevices that can create a thermal illusion. TT and SC methods can be used to tune neighboring temperature fields of the target to mimic the reference temperature field. Han *et al.*[12] was the first to design thermal metamaterials' functionality to achieve thermal camouflage based on the SC method. He and Wu[15] proposed a thermal reshaper as an illusion device. It combined a thermal amplifier, concentrator, invisible cloak, and shrinker, and was based on the TT method. Hou *et al.*[16] designed an illusion device to camouflage the location of a target theoretically and experimentally. Hu *et al.*[13] aimed to camouflage the outer and the inner temperature fields of a metadevice simultaneously using general illusion thermotics in which the conventional TT method was extended by splitting the coordinate space into two- and three-dimensional spaces.

Although TT and SC can be used to design thermal metamaterials and metadevices for diverse thermal functionalities, they suffer from inherent defects. For instance, TT is flexible and can be used for diverse thermal functionalities, though the corresponding anisotropic thermal conductivity makes devices based on TT rather complicated to fabricate and implement. In contrast, SC is easy to implement but has limited flexibility. Stimulated by the diverse functionalities and promising applications of thermal metamaterials, researchers continue to spare no effort on seeking alternative methods that can balance the complexity of design, fabrication, and application.

Topology optimization is a numerical iterative procedure for optimizing a structure. It can find the optimal distribution of

materials for some given constraints in a given design area to maximize or minimize the structural performance of a device.[17–20] So far, topology optimization has been used to design an optical cloak,[21,22] a DC current cloak,[23] and thermal cloaks.[24,25] It is another option for designing thermal metamaterials and metadevices with different thermal functionalities. Andkjær *et al.*[21] designed optical cloaks using only dielectric materials that did not rely on polarization. Lin *et al.*[26] presented a general topology optimization scheme for multi-layered geometries with angular phase control, including an angular converging metalens, which focuses light onto the same focal spot regardless of the angle of incidence, and a single-piece nanophotonic metalens with angular aberration correction. Based on topology optimization, Fujii *et al.*[24] designed optimized configurations for thermal invisibility composed of aluminum and iron. Fujii and Akimoto[25] designed thermal carpet cloaks with a topology optimization method that eliminates disturbances caused by a bump on a flat boundary. Is it possible to extend topology optimization to general illusion thermotics for broad applications in addition to TT and SC methods?

In this paper, we proposed a topology optimization scheme to design illusion thermotics for camouflaging the external temperature field. We provide a detailed introduction to the topology optimization scheme and discuss the thermal illusion performance in terms of the number, locations, and types of material of the thermal illusions. The flexibility and possible extensions of the two-material topology optimization scheme are also discussed.

II. METHODOLOGY

First, we briefly introduce the general topology optimization scheme for achieving a thermal illusion. Figure 1 illustrates the proposed scheme. A single heat source in the center of the design domain will be camouflaged as four illusion heat sources in its exterior region. The computational model with a single material (i.e., FR-4) and four illusion heat sources is shown in Fig. 1(a), and its steady temperature field is considered as a reference temperature field. The multi-material topology optimization model with a single heat source in the center domain is shown in Fig. 1(b). The fixed domain Ω_D contains two materials (iron and FR-4), which are freely distributed. The exterior domain of Ω_D is denoted by Ω_{out}. The temperature distribution depends on the layout of iron and FR-4. Both convection and temperature on the boundaries of Ω_{out} are fixed as 0 W/m^2 K and 0 K, respectively, and structural symmetries are imposed along x and y axes for simplification, as can be seen in Fig. 1.

In the topology optimization scheme of Fig. 1, when a perfect thermal illusion to be achieved,[13] the temperature field distribution of domain Ω_{out} with a single heat source, as shown in Fig. 1(b), should be identical to that of domain Ω_{out} with four illusion heat sources, as shown in Fig. 1(a). To achieve this goal, the topology of the multi-material structure shown in Fig. 1(b) is optimized. The objective function is set as

$$J = \frac{1}{J_0} \int_{\Omega_{out}} |T - T_{ref}|^2 d\Omega_{out}, \tag{1}$$

where T is the temperature in Fig. 1(b), which is to be controlled by the topology of an optimized structure. T_{ref} is the reference temperature in Fig. 1(a). The objective function J is normalized by J_0, which is defined as

$$J_0 = \int_{\Omega_{out}} |T_0 - T_{ref}|^2 d\Omega_{out}, \tag{2}$$

where T_0 is the temperature when Ω_D in Fig. 1(b) is filled with the single material FR-4. As J is minimized, T tends to T_{ref} in Ω_{out}, which means that the temperature fields in Ω_{out} are close under different heat sources. Thus, the thermal illusion is realized, i.e., we

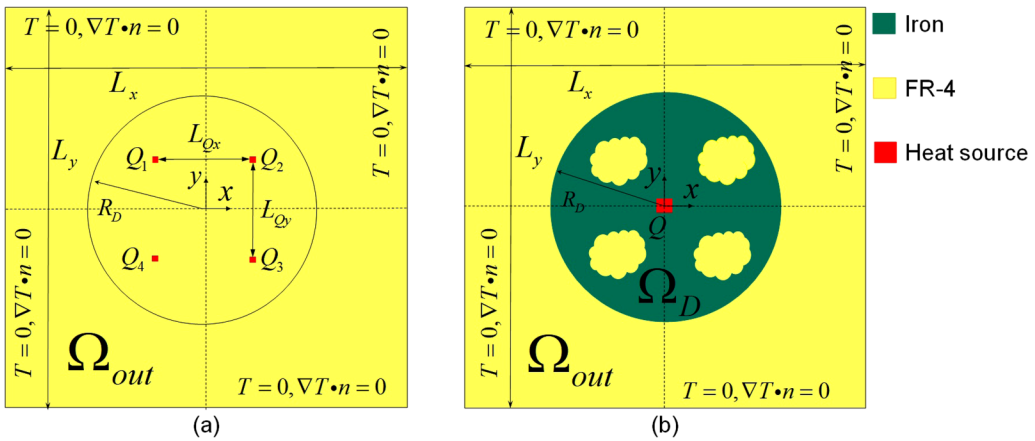

FIG. 1. (a) Computational model for the reference temperature field. (b) Topology optimization model for the temperature field with a thermal illusion device. Domain sizes are $L_x = L_y$, $R_D = L_x \times 2/7$, and $L_{Qx} = L_{Qy} = L_x \times 1/4$. The heat sources are set to $Q = Q_1 = Q_2 = Q_3 = Q_4 = 8\,\mathrm{W/m^3}$, and their areas are set to $S_Q = 4S_1 = 4S_2 = 4S_3 = 4S_4$. The thermal conductivities of FR-4 and iron are 0.3 and 56 W/m K, respectively.

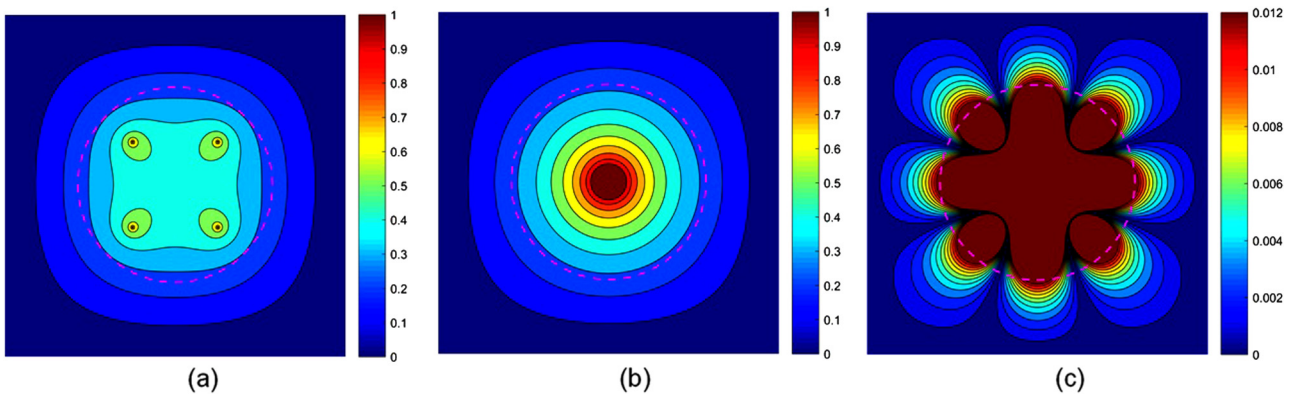

FIG. 2. (a) Normalized reference temperature of the domain with four illusion heat sources, T^n_{ref}. (b) Normalized temperature of the design domain filled with the single material FR-4 under a single heat source, T^n_0. (c) The absolute temperature difference between T^n_0 and T^n_{ref}, $|T^n_0 - T^n_{ref}|$. In Figs. 2(a)–2(c), the intervals between isotherms are 0.1, 0.1, and 0.001, respectively. The purple dotted line is the boundary of domain Ω_D.

cannot determine the position of the actual heat source in Ω_D based on measuring the exterior temperature field. The temperatures T_{ref}, T_0, and T in the steady-state thermal conduction obey the Laplace equation with heat sources,

$$\begin{aligned} \nabla(k_{ref}(x_e)\nabla T_{ref}) &= Q_1 + Q_2 + Q_3 + Q_4, \\ \nabla(k_{ref}(x_e)\nabla T_0) &= Q, \\ \nabla(k(x_e)\nabla T) &= Q, \end{aligned} \tag{3}$$

where $k_{ref}(x_e)$ and $k(x_e)$, respectively, are the thermal conductivities of the whole domain in Figs. 1(a) and 1(b). They are defined as

$$\begin{aligned} k_{ref}(x_e) &= k_{FR-4}, \\ k(x_e) &= \begin{cases} k_{FR-4} + x_e(k_{iron} - k_{FR-4}), & x_e \in \Omega_D, \\ k_{FR-4}, & x_e \in \Omega_{out}, \end{cases} \end{aligned} \tag{4}$$

where k_{FR-4} and k_{iron} denote the thermal conductivities of FR-4 and iron, respectively. In this paper, the solid isotropic material with penalization (SIMP) method is employed in the topology optimization.[27] Here, $x_e \in [0, 1]$ is the relative density design variable. After topology optimization, the intermediate densities will be removed by postprocessing. Finally, x_e can be described by

$$x_e = \begin{cases} 1, & x_e \in \text{iron}, \\ 0, & x_e \in \text{FR-4}. \end{cases} \tag{5}$$

In practice, considering the weight of the structure in Ω_D, a volume constraint is imposed on the amount of iron,

$$\int_{\Omega_D} x_e d\Omega_D \le Vf, \tag{6}$$

where V is the total volume of domain Ω_D and f is the volume fraction of iron within Ω_D. In the topology optimization of a thermal illusion, the design variables are iteratively updated using a gradient-based optimization method, i.e., the method of moving asymptotes (MMA).[28–30] The iteration is terminated when the difference in the values of the design variables between two successive iterations is less than 10^{-3} or after a maximum of 150 iteration steps. The sensitivity analysis of the objective and constraint functions is conducted by the adjoint method.[31–33]

III. RESULTS AND DISCUSSION

To simplify the comparisons, the temperatures T_{ref}, T, and T_0 are normalized as T^n_{ref}, T^n, and T^n_0 by $T^n_i = (T_i - \min(T_{ref}))/(\max(T_{ref}) - \min(T_{ref}))$, where $T_i = T_{ref}$, T, or T_0. The reference temperature field T^n_{ref} of the domain with the four illusion heat sources in Fig. 1(a) is shown in Fig. 2(a). The temperature field T^n_0 is shown in Fig. 2(b). The differences between T^n_0 and T^n_{ref} before topology optimization are shown in Fig. 2(c) to illustrate the thermal illusion more intuitively. The aim of topology optimization is that the temperature outside the device region (outside the purple dashed line) and the reference temperature are so similar that the temperature differences are negligible, which would mean that the thermal illusion has been realized by the layout of FR-4 and iron.

Figure 3 shows the results of topology optimization for a thermal illusion device with different volume fractions of iron when the number of illusion heat sources is four. Each optimized structure shown in the leftmost column of Fig. 3 is composed of FR-4 and iron. Compared to the thermal illusion structure designed by TT,[13] the configuration of each structure obtained by topology optimization is much simpler. In these optimized structures, iron, which has a high thermal conductivity, is in the domains of the single actual heat source and the four illusion heat sources. As the volume fraction of iron increases, there is a good connection between iron in the two domains. The steady temperature fields of the single heat source in the domain with the multi-material distribution are shown in the center column of Fig. 3. This is the temperature field produced for the thermal illusion by topology optimization. The differences between the temperature field T^n and the reference temperature field T^n_{ref} in the domain Ω_{out} are shown in the rightmost column of Fig. 3. These temperature differences in

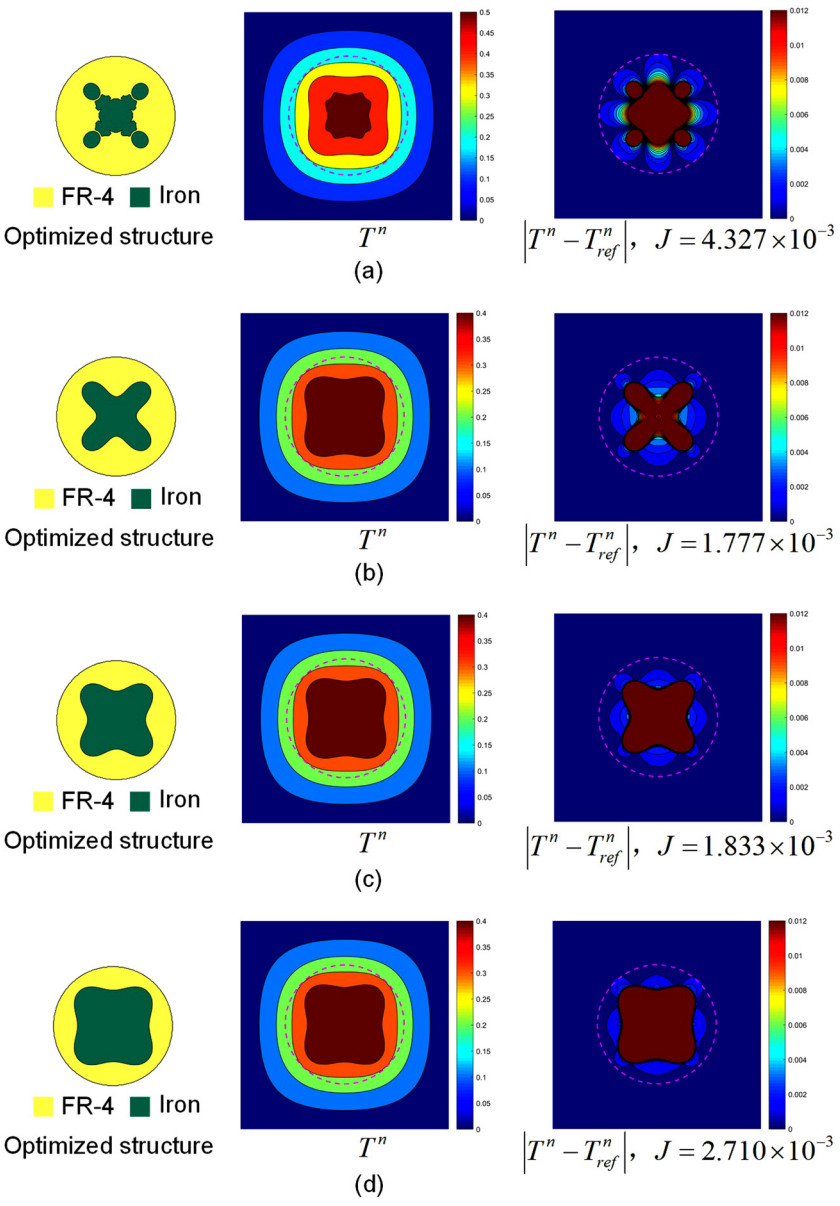

FIG. 3. Results of topology optimization used to camouflage a single heat source into four heat sources with different volume fractions of iron: (a) $f_{iron} = 0.2$, (b) $f_{iron} = 0.3$, (c) $f_{iron} = 0.4$, and (d) $f_{iron} = 0.5$. Left: topology-optimized thermal illusion structures. Center: thermal illusion temperature field. The interval between isotherms is 0.1. Right: absolute values of the differences between the thermal illusion temperature field and the reference temperature field. The interval between isotherms is 0.001. $J_0 = 1367.8248$. The purple dotted line is the boundary of the domain Ω_D.

the domain Ω_{out} are extremely small. Thus, the single heat source in the center of the design domain has been camouflaged by the four heat sources in its exterior region. Due to the negligible temperature differences between T_0^n and T_{ref}^n, the two-material topology optimization has been verified as being effective for illusion thermotics design.

In addition, the effectiveness of this thermal illusion can be evaluated using the objective function [Eq. (1)]. After topology optimization, the objective function J is minimized and its value is as low as 10^{-3}, as shown in the rightmost column of Fig. 3. This low value of the objective function J means that the temperature field in domain Ω_{out} is very close to the reference one. This further illustrates that the single actual heat source can be camouflaged as four virtual illusion heat sources using two-material topology optimization. Therefore, based on the exterior temperature field in the domain Ω_{out}, it is difficult to judge the number of actual heat sources. Moreover, the temperature changes around the center of the domain Ω_D are so small that we cannot determine whether the single actual heat source is in the center of Ω_D. This further demonstrates the effectiveness of the thermal illusion of the single actual heat source. Thus, the steady temperature field with the single actual heat source in the center of Ω_D will provide misleading information if we attempt to detect the number and location of the actual heat sources through infrared imaging.

To assess the flexibility of topology optimization for illusion thermotics, different reference temperature fields with different numbers of illusion heat sources and asymmetric illusion heat sources were investigated for the same design domain. The results of topology optimization are shown in Fig. 4. For Figs. 4(a)–4(c), the distance from each illusion heat source to the center of the design domain is $L_x/4$. The illusion heat sources are at the vertexes of a triangle, square, and hexagon, respectively. For Fig. 4(d), the four illusion heat sources are asymmetric. The illusion heat sources in Fig. 4 have the same density. The total volume of all the illusion heat sources in each case is equal to that of the single heat source in Fig. 1(b). For each of the optimized structures shown in the leftmost column of Fig. 4, it can be observed that iron is distributed in the domain of the single actual heat source and the camouflaged or illusion heat sources after topology optimization. Moreover, as shown in the rightmost column of Fig. 4, the objective function is very small and the temperature field in Ω_{out} after topology optimization is very close to the reference one. Hence, a thermal illusion for each of these cases can be realized by two-material topology optimization. As before, the temperature changes around the center of the domain Ω_D are very small, which further indicates that the single actual heat source has been camouflaged by different multiple heat sources. Topology optimization can be used to design different optimized structures according to the requirements of the thermal illusion.

Furthermore, the topology optimization method presented can be extended to use a wider range of materials. We replaced iron with stainless steel (17 W/m K) or wood (0.5 W/m K), which have a lower thermal conductivity, to test the effectiveness of topology optimization. The other numerical test conditions are consistent with those in Fig. 1. The reference temperature field in Fig. 2(a) was used. The results of the topology optimization are shown in Fig. 5. The objective function and the temperature differences are shown in the third column of Fig. 5, which indicate that the thermal illusion has been realized by topology optimization with different materials. The temperature differences in Ω_{out}, as shown in Fig. 5(c), are extremely small and the objective function is as low as 10^{-5}, which demonstrates the effectiveness of the thermal illusion.

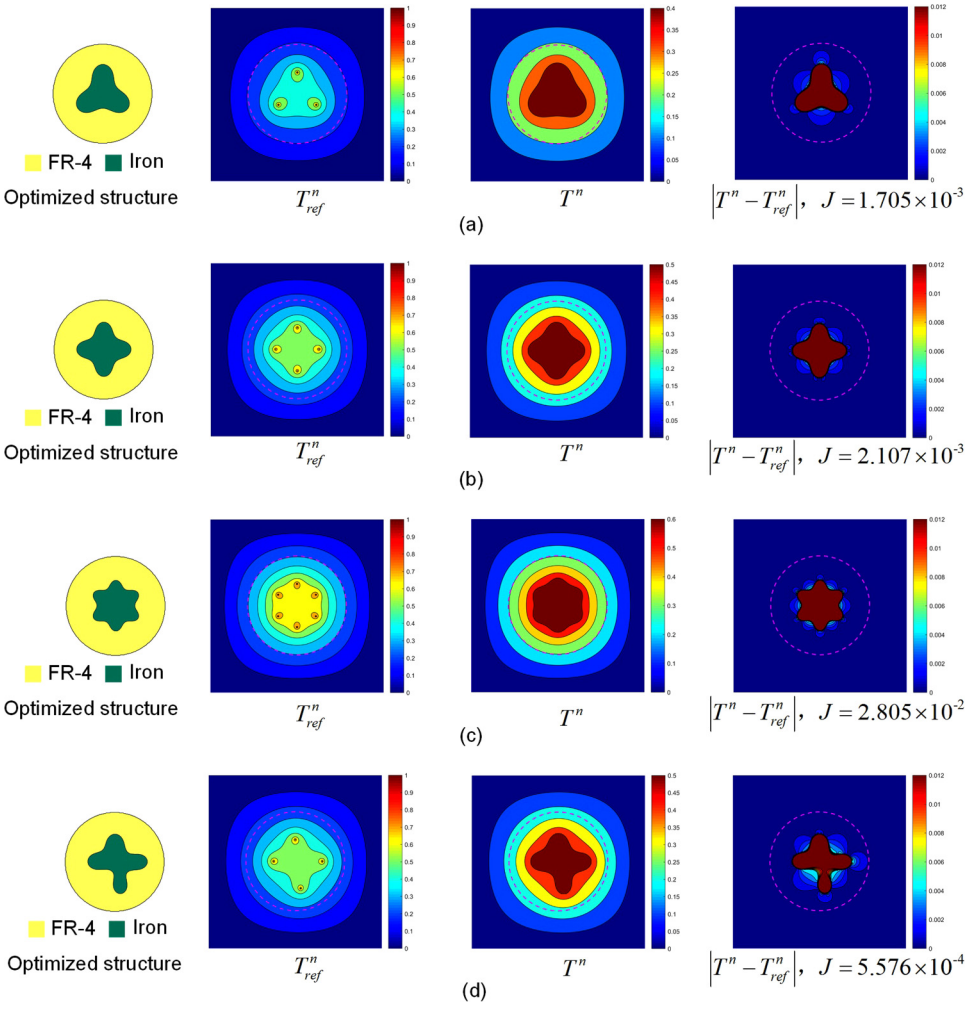

FIG. 4. Results of topology optimization used to camouflage a single heat source into (a) three, (b) four, (c) six symmetric illusion, and (d) four asymmetrical illusion heat sources with the volume fractions of iron $f_{iron} = 0.2$. Left: topology-optimized thermal illusion structures. Second column: the reference temperature field. The interval of between isotherms is 0.1. Third column: thermal illusion temperature field. The interval of between isotherms is 0.1. Right: absolute values of the differences between the thermal illusion temperature field and the reference temperature field. The interval between isotherms is 0.001. Under each case, $J_0 = 993.057$, 85.3695, 2.2158, and 4271.1506, respectively. The purple dotted line is the boundary of domain Ω_D.

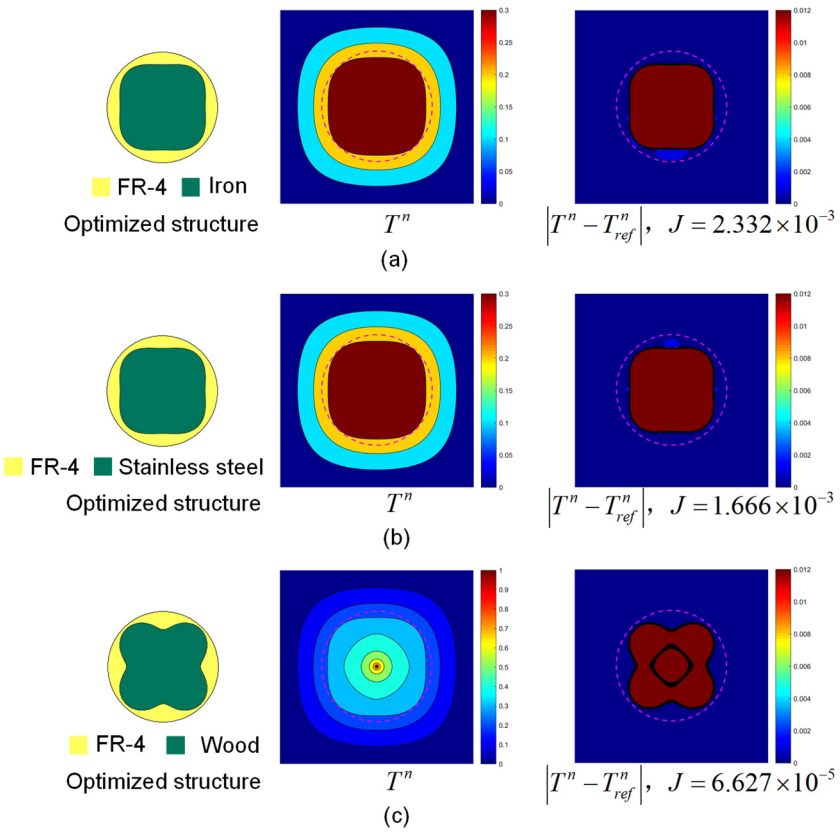

FIG. 5. Results of topology optimization used to camouflage a single heat source into four heat sources under different materials: (a) iron and FR-4, (b) stainless steel and FR-4, and (c) Wood and FR-4. Left: topology-optimized thermal illusion structures. Center: thermal illusion temperature field. The interval between isotherms is 0.1. Right: absolute values of the differences between the thermal illusion temperature field and the reference temperature field. The interval between isotherms is 0.001. The volume fraction of the material with relatively high thermal conductivity is set as 0.7 and $J_0 = 1367.8248$. The purple dotted line is the boundary of domain Ω_D.

In previous demonstrations of illusion thermotics, a single heat source was camouflaged into multiple illusions, but the topology optimization method presented can also be extended to camouflaging multiple heat sources with one or multiple illusions. This is one of the advantages of this method over TT or SC methods. To demonstrate this, as shown in Fig. 6, four heat sources were camouflaged by two illusion ones by changing the reference heat sources and actual heat sources following the same topology optimization procedure. The reference temperature field T^n_{ref} of the domain with two illusion heat sources is shown in Fig. 6(a). The field T^n_0 of the four heat sources is shown in Fig. 6(b). For comparison, the temperature differences between them are shown in Fig. 6

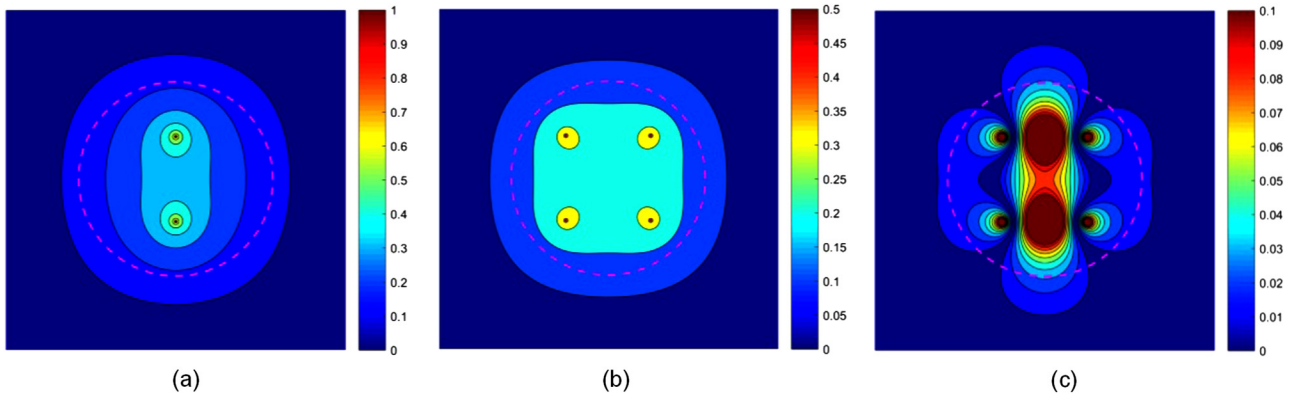

FIG. 6. (a) Normalized reference temperature of the domain with two illusion heat sources, T^n_{ref}. (b) Normalized temperature of the design domain filled with the single material FR-4 and four heat sources, T^n_0. (c) The absolute temperature difference between T^n_0 and T^n_{ref}, $|T^n_0 - T^n_{ref}|$. In Figs. 6(a)–6(c), the interval between isotherms are 0.1, 0.1, and 0.001, respectively. The purple dotted line is the boundary of domain Ω_D.

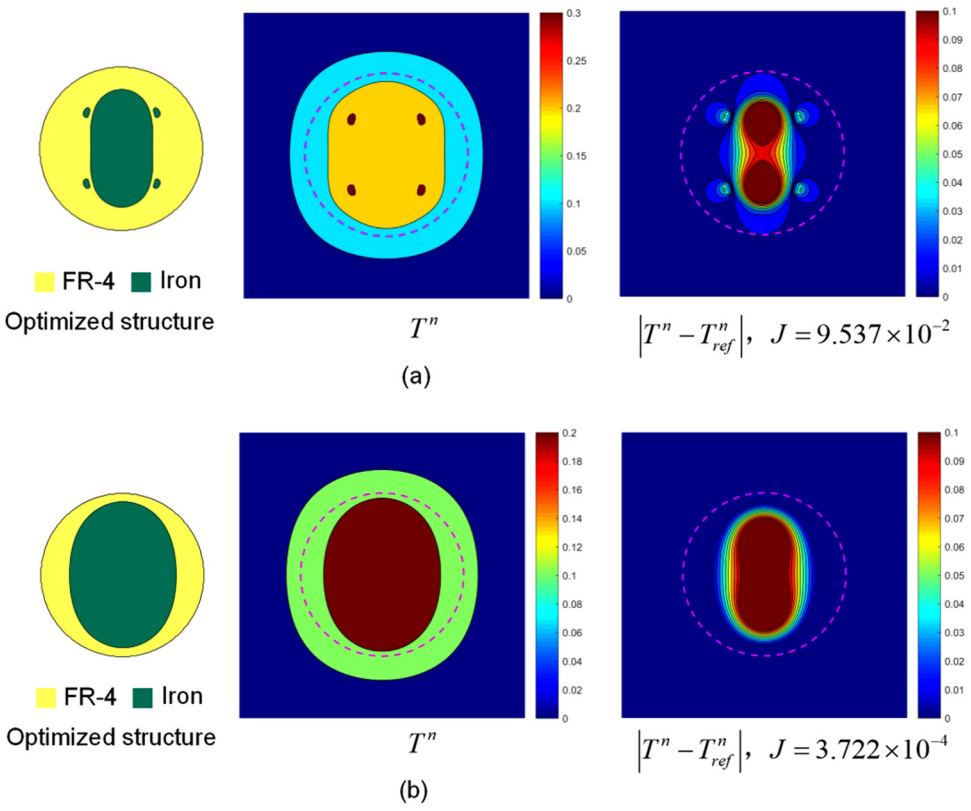

FIG. 7. Results of topology optimization used to camouflage four actual heat sources into two illusion ones. Left: topology-optimized thermal illusion structures. Center: thermal illusion temperature field. The interval between isotherms is 0.1. Right: absolute values of the differences between the thermal illusion temperature field and the reference temperature field. The interval between isotherms is 0.001. Under each case, (a) $f_{iron} = 0.3$, $J_0 = 13\ 297.0329$ and (b) $f_{iron} = 0.6$, $J_0 = 13\ 297.0329$, respectively. The purple dotted line is the boundary of domain Ω_D.

(c). After topology optimization, the results of thermal illusion are shown in the rightmost column of Fig. 7. The leftmost column of Fig. 7 indicates how the different volume fractions of iron in the topology-optimized structures are distributed in the domain of the single actual heat source and the camouflaged or illusion heat sources. As seen in the rightmost column of Fig. 7, the temperature differences in Ω_{out} and the objective function are extremely small. Therefore, the thermal illusion has been well realized by appropriately distributing iron in FR-4.

Note that all the above thermal illusions were realized in two dimensions. Nevertheless, it is easy to extend the thermal illusion scheme to three dimensions. In three-dimensional thermal illusion, the actual heat source can be camouflaged by virtual heat sources in more directions, which can obviously enhance the effectiveness of the thermal illusion. Note that the thermal illusion scheme in this paper was verified by numerical simulations only. Since the optimized structures are simple and need only two types of material, they can be fabricated with laser processing, 3D printing, etc. Thus, the temperature fields could be observed experimentally, after imposing the relevant thermal boundary conditions on the structures.

IV. CONCLUSIONS

In summary, we proposed a general topology optimization method for designing thermal illusion devices with steady heat conduction by distributing two materials with different thermal conductivities. For the optimized structures designed by this method, the exterior thermal signature of the real heat source is close to the exterior reference thermal signature for multiple asymmetric and symmetric illusion heat sources. In the illusion, it appears as if the interior real heat source has been split. This topology optimization method is general and can be extended to other target illusions, materials, structures, boundary conditions, etc. The topology optimization method presented could be applied to the development of multi-functional illusions in other physical fields, such as optics, acoustics, and mechanics.

ACKNOWLEDGMENTS

This research was supported by the National Natural Science Foundation of China (NNSFC) (Grant No. 51606074), the Natural Science Foundation of Hubei Province (Grant No. 2019CFA059), the Program for HUST Academic Frontier Youth Team (Grant No. 2017QYTD04), and the Open Projects Foundation of Yangtze Optical Fiber and Cable Joint Stock Limited Company (Grant No. SKLD1708).

DATA AVAILABILITY

The data that support the findings of this study are available from the corresponding author upon reasonable request.

REFERENCES

[1]R. Hu, S. Huang, M. Wang, X. Luo, J. Shiomi, and C. Qiu "Encrypted thermal printing with regionalization transformation," Adv. Mater. **31**, 1807849 (2019).
[2]J. Song, S. Huang, Y. Ma, Q. Cheng, R. Hu, and X. Luo, "Radiative metasurface for thermal camouflage, illusion and messaging," Opt. Express **28**, 875–885 (2020).
[3]R. Hu, Y. Liu, S. Shin, S. Huang, X. Ren, W. Shu, J. Cheng, G. Tao, W. Xu, R. Chen, and X. Luo, "Emerging materials and strategies for personal thermal management," Adv. Energy Mater. **10**, 1903921 (2020).
[4]S. Guenneau, C. Amra, and D. Veynante, "Transformation thermodynamics: Cloaking and concentrating heat flux," Opt. Express **20**, 8207 (2012).
[5]R. Hu, S. Iwamoto, L. Feng, S. Ju, S. Hu, M. Ohnishi, N. Nagai, K. Hirakawa, and J. Shiomi, "Machine-learning-optimized aperiodic superlattice minimizes coherent phonon heat conduction," Phys. Rev. X **10**, 021050 (2020).
[6]R. Hu and X. Luo, "Two-dimensional phonon engineering triggers microscale thermal functionalities," Natl. Sci. Rev. **6**, 1071–1073 (2019).
[7]S. Narayana and Y. Sato, "Heat flux manipulation with engineered thermal materials," Phys. Rev. Lett. **108**, 214303 (2012).
[8]R. Hu, J. Song, Y. Liu, W. Xi, Y. Zhao, X. Yu, Q. Cheng, G. Tao, and X. Luo, "Machine learning-optimized Tamm emitter for high-performance thermophotovoltaic system with detailed balance analysis," Nano Energy **72**, 104687 (2020).
[9]C. Z. Fan, Y. Gao, and J. P. Huang, "Shaped graded materials with an apparent negative thermal conductivity," Appl. Phys. Lett. **92**, 251907 (2008).
[10]R. Hu, X. L. Wei, J. Y. Hu, and X. B. Luo, "Local heating realization by reverse thermal cloak," Sci. Rep. **4**, 3600 (2014).
[11]F. Chen and D. Y. Lei, "Experimental realization of extreme heat flux concentration with easy-to-make thermal metamaterials," Sci. Rep. **5**, 11552 (2015).
[12]T. Han, X. Bai, J. T. L. Thong, B. Li, and C. W. Qiu, "Full control and manipulation of heat signatures: Cloaking, camouflage and thermal metamaterials," Adv. Mater. **26**, 1731 (2014).
[13]R. Hu, S. L. Zhou, Y. Li, D. Y. Lei, X. B. Luo, and C. W. Qiu, "Illusion thermotics," Adv. Mater. **30**, 1707237 (2018).
[14]X. Peng and R. Hu, "Three-dimensional illusion thermotics with separated thermal illusions," ES Energy Environ. **6**, 39–44 (2019).
[15]X. He and L. Wu, "Illusion thermodynamics: A camouflage technique changing an object into another one with arbitrary cross section," Appl. Phys. Lett. **105**, 221904 (2014).
[16]Q. Hou, X. Zhao, T. Meng, and C. Liu, "Illusion thermal device based on material with constant anisotropic thermal conductivity for location camouflage," Appl. Phys. Lett. **109**, 103506 (2016).
[17]O. Sigmund, "A 99-line topology optimization code written in Matlab," Struct. Multidiscip. Optim. **21**, 120 (2001).
[18]J. Gao, H. Li, L. Gao, and M. Xiao, "Topological shape optimization of 3D micro-structured materials using energy-based homogenization method," Adv. Eng. Softw. **116**, 89 (2018).
[19]Y. Zhang, M. Xiao, X. Zhang, and L. Gao, "Topological design of sandwich structures with graded cellular cores by multiscale optimization," Comput. Methods Appl. Mech. Eng. **361**, 112749 (2020).
[20]Y. Wang, H. Xu, and D. Pasini, "Multiscale isogeometric topology optimization for lattice materials," Comput. Methods Appl. Mech. Eng. **316**, 568–585 (2017).
[21]J. Andkjær, N. Asger Mortensen, and O. Sigmund, "Towards all-dielectric, polarization-independent optical cloaks," Appl. Phys. Lett. **100**, 101106 (2012).
[22]G. Fujii, H. Watanabe, T. Yamada, T. Ueta, and M. Mizuno "Level set based topology optimization for optical cloaks," Appl. Phys. Lett. **102**, 251106 (2013).
[23]G. Fujii, Y. Akimoto, and M. Takahashi, "Direct-current electric invisibility through topology optimization," J. Appl. Phys. **123**, 233102 (2018).
[24]G. Fujii, Y. Akimoto, and M. Takahashi, "Exploring optimal topology of thermal cloaks by CMA-ES," Appl. Phys. Lett. **112**, 061108 (2018).
[25]G. Fujii and Y. Akimoto, "Topology-optimized thermal carpet cloak expressed by an immersed-boundary level-set method via a covariance matrix adaptation evolution strategy," Int. J. Heat Mass Transfer **137**, 1312–1322 (2019).
[26]Z. Lin, B. Groever, F. Capasso, W. A. Rodriguez, and M. Lončar, "Topology-optimized multilayered metaoptics," Phys. Rev. Appl. **9**, 044030 (2018).
[27]E. Andreassen, A. Clausen, M. Schevenels, B. S. Lazarov, and O. Sigmund, "Efficient topology optimization in MATLAB using 88 lines of code," Struct. Multidiscip. Optim. **43**, 1 (2011).
[28]K. Svanberg, "The method of moving asymptotes—A new method for structural optimization," Int. J. Numer. Methods Eng. **24**, 359 (1987).
[29]Y. Zhang, L. Gao, and M. Xiao, "Maximizing natural frequencies of inhomogeneous cellular structures by Kriging-assisted multiscale topology optimization," Comput. Struct. **230**, 106197 (2020).
[30]Y. Zhang, M. Xiao, L. Gao, J. Gao, and H. Li, "Multiscale topology optimization for minimizing frequency responses of cellular composites with connectable graded microstructures," Mech. Syst. Signal. Process. **135**, 106369 (2020).
[31]J. S. Jensen and O. Sigmund, "Topology optimization of photonic crystal structures: A high-bandwidth low-loss T-junction waveguide," J. Opt. Soc. Am. B **22**, 1191 (2005).
[32]S. Chu, L. Gao, M. Xiao, and Y. Zhang, "Multiscale topology optimization for coated structures with multifarious-microstructural infill," Struct. Multidiscip. Optim. **61**, 1473 (2020).
[33]S. Chu, L. Gao, M. Xiao, Z. Luo, "Stress-based multi-material topology optimization of compliant mechanisms," Int. J. Numer. Methods Eng. **113**, 1021 (2018).